ISBN: 978-3-95450-247-9 ISSN: 2673-5490 doi: 10.18429/JACoW-IPAC2024-WEPG38

GEANT4 SIMULATIONS ON FARADAY CUP DESIGN FOR PIP-II LASER WIRE SCANNER SYSTEM *

S. A. K. Wijethunga †, R. M. Thurman-Keup, V. E. Scarpine
Fermi National Accelerator Laboratory, Batavia, Illinois, USA

Abstract

The Proton Improvement Plan-II (PIP-II) accelerator upgrade at Fermilab represents a groundbreaking leap forward in high-energy physics research. This ambitious initiative involves enhancing Fermilab's accelerator complex by replacing the current linear accelerator (linac) with a warm front end (WFE) capable of accelerating H^- beams up to 2.1 MeV. Subsequently, a superconducting linac further accelerates these beams up to 800 MeV. To precisely measure the transverse beam profile, a combination of traditional wire scanners at the WFE section and Laser wire scanners along the superconducting linac are planned for implementation. This investigation is centered on refining the Faraday cup design for the PIP-II Laser wire scanners by utilizing GEANT4, a Monte Carlo simulation toolkit. Leveraging this method enables a comprehensive analysis of particle trajectories, energy deposition, secondary particle emission, backscattering, etc., facilitating optimization through adjustments to cup geometries, materials, and placement to maximize its efficacy in beam diagnostics.

INTRODUCTION

The Fermilab Proton Improvement Plan-II (PIP-II) stands as a significant upgrade project designed to elevate the performance of Fermilab's accelerator complex. A primary objective of the PIP-II linac is to substantially boost the energy of the H^- beam from 400 MeV to 800 MeV, surpassing the capabilities of the current linac. In pursuit of these objectives, while maximizing cost-effectiveness, the plan involves implementing superconducting radiofrequency (SRF) technology. The final linac design comprises a warm front end featuring a low energy beam transport (LEBT) section, followed by an RFQ, and further by a medium energy beam transport (MEBT) section, which ramps up the energy to 2.1 MeV. Subsequently, a superconducting linac (SCL) equipped with five distinct SRF cavity types facilitates the acceleration to the final 800 MeV [1].

However, beam profile measurements pose a challenge within the high vacuum levels necessitated by the SCL. The conventional wire scanner method proves impractical due to concerns surrounding particle contamination, vacuum degradation, and resultant beam loss, leading to issues such as heating and quenching. Therefore, a non-invasive approach to beam profile measurement, such as substituting the carbon wire scanner with a laser wire scanner, is being considered. This methodology has already been successfully employed at the Spallation Neutron Source (SNS) at Oak Ridge National Laboratory (ORNL) [2].

The principle of the laser wire profile measurement is based on photoionization, as shown in Eq. 1.

$$H^- + \gamma \rightarrow H^0 + e^- \quad (1)$$

When the Laser intercepts with the H^- beam at a certain wavelength, it causes electrons to detach from the H^-. The density of the H^- beam can be determined by measuring the density of the detached electrons [3].

Figure 1 illustrates the Laser wire scanner system. It primarily involves a laser wire system, a deflecting magnet to divert the detached electrons away from the H^- beam, and a Faraday cup (FC) to collect those electrons. There are 13 laser wire stations located along the 200 m long SCL, first at 2.1 MeV and last at 800 MeV.

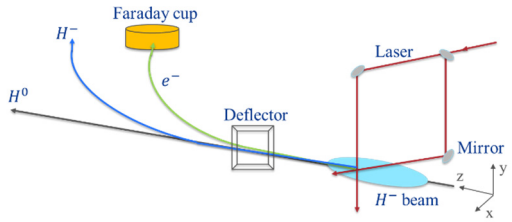

Figure 1: Laser wire scanner system.

The FC stands out as a straightforward, easily handled, and cost-effective solution for accurately measuring absolute beam current. Careful consideration of the FC's physical properties is key to minimizing signal losses. Factors such as geometry, material nature, and target wall thickness are crucial in the FC design. Further, challenges arise due to phenomena like secondary electron emission and backscattering, which can lead to inaccuracies in beam current measurements. Therefore, understanding these phenomena and optimizing the FC design accordingly is essential for achieving accurate measurements [4-6].

In this paper, we outline the design concept of the FC and describe simulations conducted to better understand the stated phenomena. We utilize Geant4, a well-known toolkit recognized for its Monte Carlo simulations of particle interactions with matters.

DESIGN CONCEPT

The initial design steps prioritize the selection of material and determining the cup thickness. To minimize electron leakage, the cup thickness must exceed the penetration depth of incident electrons. To decide on the appropriate thickness, the electron stopping distance was computed for several potential FC materials, including Cu, Al, W,

* This manuscript has been authored by Fermi Research Alliance, LLC under Contract No. DE-AC02-07CH11359 with the U.S. Department of Energy, Office of Science, Office of High Energy Physics.
† swijethu@fnal.gov

ISBN: 978-3-95450-247-9 ISSN: 2673-5490 doi: 10.18429/JACoW-IPAC2024-WEPG38

Stainless steel, and Mb. This calculation utilized the Continuous Slowing Down Approximation (CSDA) range for each material [7]. Figure 2 illustrates the relationship between the stopping distance derived from the CSDA range and the kinetic energy for the materials under consideration.

In this investigation, we examined FCs positioned at the first and last Laser wire scanner locations, corresponding to H^- beam energies of 2.1 MeV and 800 MeV, respectively. Consequently, the energy of the detached electrons was calculated to be 1 keV at first and 450 keV at the last Laser wire locations. As depicted in Figure 2, the electron stopping distance for Cu, W, Stainless steel, and Mb is below 0.25 mm for 450 keV electrons, and it should be considerably smaller for 1 keV electrons. However, we chose to primarily focus on Cu for its exceptional electrical and thermal properties, and Stainless steel for its ease of use and safety in the sensitive vacuum environment.

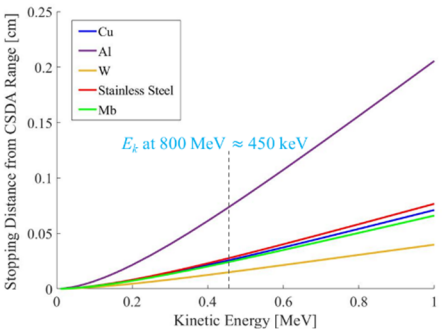

Figure 2: Stopping distance from CSDA range for different materials as a function of electron kinetic energy.

The next focus of the design is to optimize the geometry that could be accommodated within the limited space available for beam instrumentation devices situated between the cryomodules of the superconducting linac. A stopping distance of 0.25 mm offers ample flexibility in selecting the thickness of the cup for both Cu and Stainless steel materials.

Figure 3 illustrates the considered Laser wire scanner setup (near the Laser interaction point) and its cross-section with anticipated electron trajectory.

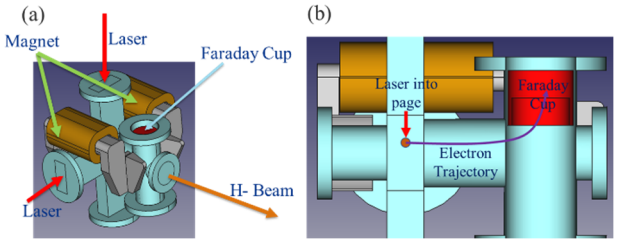

Figure 3: (a) Illustration of the Laser wire scanner setup near the interaction point. (b) Cross-section of the setup indicating the anticipated electron trajectory.

As shown in the figure, deflecting magnets are pivotal in guiding the electrons into the FC. These magnets were designed using CST software, incorporating angled pole pieces to generate a quadrupole field, thereby preventing electron dispersion in the transverse direction.

Based on the provided parameters, a FC was designed as illustrated in Figure 4. Given the constrained space (< 5 cm), the cup's design was chosen to be a cylindrical slab with a 5 cm diameter and 2.5 cm thickness, accompanied by a 1 cm high outer ring.

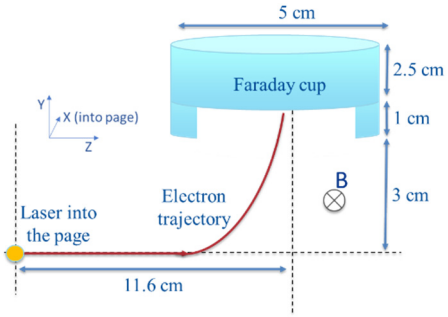

Figure 4: Schematic diagram of the FC design.

GEANT4 SIMULATIONS

To investigate the interaction of electrons with materials and the impact of secondary particles and backscattering on measurements, Geant4 simulation was employed [8, 9]. This involved utilizing physics processes such as bremsstrahlung, ionization and multiple scattering, pair production, Compton scattering, and photo-electric effect. For an accurate modeling of electromagnetic interactions at lower energy levels, two EM physics lists (constructors) were chosen: G4EmStandardPhysics_option4, which includes Goudsmit Saundeson (GS) multiple scattering for 450 keV electrons, and both G4EmStandardPhysics_option4 and G4EmStandardPhysicsSS (single scattering) for 1 keV electrons [10].

Figure 5 illustrates the Geant4 model of the FC, displaying the magnetic field area of the deflecting magnets for 450 keV electrons. Additionally, it visualizes the trajectories of electrons within the cup volume and the secondary photons.

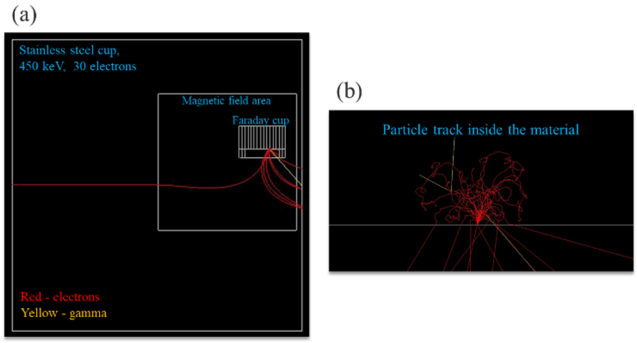

Figure 5: Visualization by Geant4 (a) the FC system, (b) particle tracks inside the material.

Figure 6 illustrates the simulation results for 450 keV electrons with a production cut value for secondaries at 0.1 mm and a step limit of 5 µm (a) Energy deposited in the cup, (b) Energy of the reflected charged particles, (c) Energy of charged secondary particle at creation, and (d) Energy of reflected neutral particles.

ISBN: 978-3-95450-247-9 ISSN: 2673-5490 doi: 10.18429/JACoW-IPAC2024-WEPG38

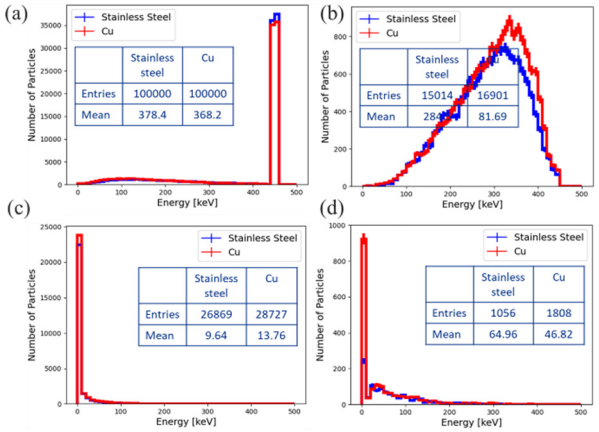

Figure 6: For 450 keV electrons (a) Energy deposited in the cup. (b) Energy of the reflected charged particles. (c) Energy of charged secondary particle at creation. (d) Energy of reflected neutral particles.

Based on the results, all particles experienced an impact on both Cu and Stainless steel materials. The calculated backscattering coefficients were found to be 17% for Cu and 15% for Stainless steel, which is lower than the standard backscattering coefficient [11, 12] for these materials, possibly due to the recapture of backscattered electrons by the magnetic field. As shown in Figure 6 (c), the kinetic energy of the secondary electrons is small; thus, the Larmour radius can be kept small with a relatively low magnetic field. Additionally, the analysis revealed that 28.7% and 26.8% of charged secondary particles were generated for Cu and Stainless steel, respectively. Furthermore, simulations showed all reflected particles were primary particles, and no particles were transmitted through the cup.

Similarly, Figure 7 illustrates the simulation results for 1 keV electron with a production cut value for secondaries at 0.01 mm and a step limit of 1 µm (a) Energy deposited in the cup. (b) Energy of the reflected charged particles.

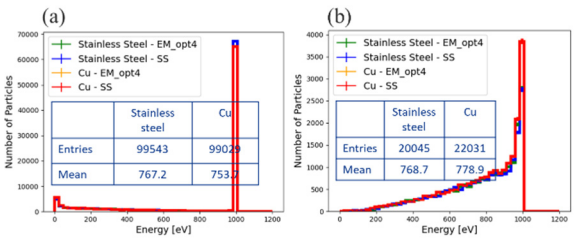

Figure 7: For 1 keV electrons (a) Energy deposited in the cup. (b) Energy of the reflected charged particles.

The results reveal that both G4EmStandardPhysics_option4 and G4EmStandardPhysicsSS yield comparable outcomes at low energies. Additionally, nearly all electrons impacted both materials. The backscattering coefficient was determined to be 22% for Cu and 22% for Stainless steel, which is lower than standard values at this energy range, potentially due to the previously mentioned reasons. Moreover, no secondary particles were generated, and no neutral particles were reflected. Similarly, all reflected particles were primary particles, and no particles were transmitted through the cup.

Next, the electron collection efficiency along the FC diameter was simulated by changing the initial electron beam location from +15 mm above the beampipe center to -7.5 mm below the beampipe center, and the impacted and reflected electron percentage was calculated as shown in Table 1. The error of the reflected particles was calculated to be 2.5%.

Table 1: Impacted and Reflected Percentage for Both 450 kV and 1 keV Electrons at Different Beam Positions

Electron beam position [mm]	450 keV		1 keV	
	Impacted [%]	Reflected [%]	Impacted [%]	Reflected [%]
-7.5	100	15.58	99.49	21.08
-5.0	100	14.98	99.48	20.47
-2.5	100	14.98	99.47	19.86
0	100	14.88	99.46	19.47
+2.5	100	14.63	99.58	19.10
+5.0	100	14.76	99.65	19.39
+7.5	100	14.58	99.65	18.78
+10.0	100	14.61	99.56	17.96
+12.5	100	14.72	99.66	17.88
+15.0	100	14.77	99.58	16.74

The results indicate that the impact efficiency remains constant across the FC for both 1 keV and 450 keV electrons. However, the reflected (backscattered) coefficient decreases as the position of the electron beam shifts from -7.5 mm to +15 mm. This decrease occurs because, at +15 mm, the number of recaptured particles from the magnetic field is higher compared to when the beam is positioned at -7.5 mm as they reach the far edge of the FC.

SUMMARY

Geant4 simulations have been instrumental in understanding backscattered particles and secondary electrons, which are crucial for accurate measurements of a FC for the PIP-II Laser wire scanner system. Both Stainless steel and Cu yielded similar results, but Stainless steel was chosen for its suitability in vacuum environments. The current FC design demonstrates nearly 100% collection efficiency, making it suitable for accurate profile measurements. The design also shows no reflection of secondary electrons and an almost steady reflection coefficient along the cup surface, ensuring consistent measurements regardless of the interaction point. Future simulations will explore different energies along the SCL to further refine and optimize the measurement process.

ACKNOWLEDGMENT

We are grateful to Soon Yung Jun (Fermilab) and Dinupa Nawarathne (NMSU).

ISBN: 978-3-95450-247-9 ISSN: 2673-5490 doi: 10.18429/JACoW-IPAC2024-WEPG38

REFERENCES

[1] E. Prebys *et al.*, "Long Term Plans to Increase Fermilab's Proton Intensity to Meet the Needs of the Long Baseline Neutrino Program", in *Proc. IPAC'16*, Busan, Korea, May 2016, pp. 1010-1013. doi:10.18429/JACoW-IPAC2016-TUOAA03

[2] Y. Liu *et al.*, "Laser wire beam profile monitor in the spallation neutron source (SNS) superconducting linac," *Nucl. Instrum. Methods Phys. Res., Sect. A*, vol. 612, no. 2, pp. 241–253, Jan. 2010. doi:10.1016/j.nima.2009.10.061

[3] Y. Liu, C. Long, C. Peters, and A. Aleksandrov, "Measurement of ion beam profiles in a superconducting linac with a laser wire," *Applied Optics*, vol. 49, no. 35, p. 6816, Dec. 2010. doi:10.1364/ao.49.006816

[4] U. Raza *et al.*, "Faraday Cup for high current and duty cycle electron LINACs," *Bull. Soc. Vac. Coaters*, vol. 175, p. 109242, May 2020. doi:10.1016/j.vacuum.2020.109242

[5] J. Harasimowicz and C. P. Welsch, "Faraday Cup for Low-Energy, Low-Intensity Beam Measurements at the USR", in *Proc. BIW'10*, Santa Fe, NM, USA, May 2010, paper TUPSM048, pp. 257-259.

[6] R. Connolly, L. DeSanto, C. Degen, R. J. Michnoff, M. G. Minty, and D. Raparia, "A Laser-Wire Beam-Energy and Beam-Profile Monitor at the BNL Linac", in *Proc. PAC'11*, New York, NY, USA, Mar.-Apr. 2011, paper MOP194, pp. 456-458.

[7] ESTAR, https://physics.nist.gov/PhysRefData/Star/Text/ESTAR.html

[8] J. Allison *et al*., "Recent Developments in Geant4," *Nucl. Instrum. Meth. A*, vol. 835, pp. 186-225, Nov. 2016. doi:10.1016/j.nima.2016.06.125

[9] J. Allison et al., "Geant4 Developments and Applications," *IEEE Trans. Nucl. Sci*., vol. 53, pp. 270-278, Feb 2006. doi: 10.1109/TNS.2006.869826

[10] Q. Gibaru, C. Inguimbert, P. Caron, M. Raine, D. Lambert, and J. Puech, "Geant4 physics processes for microdosimetry and secondary electron emission simulation: Extension of MicroElec to very low energies and 11 materials (C, Al, Si, Ti, Ni, Cu, Ge, Ag, W, Kapton and SiO2)," *Nucl. Instrum. Methods Phys. Res., Sect. B*, vol. 487, pp. 66–77, Jan. 2021. doi:10.1016/j.nimb.2020.11.016

[11] S. H. Kim *et al.*, "Validation Test of Geant4 Simulation of Electron Backscattering," *IEEE Trans. Nucl. Sci.*, vol. 62, no. 2, pp. 451–479, Apr. 2015. doi:10.1109/tns.2015.2401055

[12] P. Dondero, A. Mantero, V. Ivanchencko, S. Lotti, T. Mineo, and V. Fioretti, "Electron backscattering simulation in Geant4," *Nucl. Instrum. Methods Phys. Res., Sect. B*, vol. 425, pp. 18–25, Jun. 2018. doi:10.1016/j.nimb.2018.03.037